A Processing Platform for Optoelectronic/Optogenetic Retinal Prosthesis

Walid Al-Atabany*, Brian McGovern, Kamyar Mehran, Rolando Berlinguer-Palmini, and Patrick Degenaar

***Abstract*—The field of retinal prosthesis has been steadily developing over the last two decades. Despite the many obstacles, clinical trials for electronic approaches are in progress and already demonstrating some success. Optogenetic/optoelectronic retinal prosthesis may prove to have even greater capabilities. Although resolutions are now moving beyond recognition of simple shapes, it will nevertheless be poor compared to normal vision. If we define the aim to be to return mobility and natural scene recognition to the patient, it is important to maximize the useful visual information we attempt to transfer. In this paper, we highlight a method to simplify the scene, perform spatial image compression, and then apply spike coding. We then show the potential for translation on standard consumer processors. The algorithms are applicable to all forms of visual prosthesis, but we particularly focus on optogenetic approaches.**

***Index Terms*—Augmented vision, channelrhodopsin, optoelectronics, optogenetics, retinal prosthesis, scene enhancement, visual prosthesis.**

I. Introduction

THE restoration of vision to patients suffering from incurable blinding diseases is a remarkable challenge being addressed by several research groups across the world. Recent patient trials have demonstrated that intraocular electrical stimulation using retinal implants can return a form of basic vision based on phosphene percept [1], [2]. This has been sufficient to enable subjects to perform simple tasks such as reading single, large, and high contrast letters and shapes. Such demonstrations provide hope that one day, functional vision can be returned with this technique.

Retinal prosthesis is primarily aimed at patients blinded by outer retinal diseases, particularly retinitis pigmentosa (RP), a class of hereditary disorders affecting ∼1:4000 [3]. It causes dysfunction of the rod photoreceptors, resulting in nightblindness, tunnel vision, and, eventually, for some patients total blindness. Numerous treatments are under investigation for RP including neurotropic factors for photoreceptor protection, retinal transplant, stem cell, treatment for macular oedema. Perhaps the most promising is gene therapy [4]. So far, efficacy has been shown for single gene defects such as RPE65 [5], but RP has clusters of involved genes that make it much more difficult to treat [6]. Consequently, there is currently no effective treatment available for this condition.

In the 1990s, Stone *et al*. [7] discovered that the retinal ganglion cells (RGCs) were still intact in RP patients, even after the onset of full blindness. This formed the basis for subsequent work on electrical retinal prosthesis targeting RGCs.

The quality of prosthetic vision is determined by the number of pixels, where they are placed, and their ability to stimulate a signal the brain can understand. Simulations of pixelized vision have suggested that at least several hundred electrodes are needed to perform useful visual functions such as navigation or face recognition [8]. In particular, Cha *et al*. [9], [10] suggested, from measurement of simulated pixelized vision with normally sighted subjects, that a 25×25 pixel array produced a vision with field of view of 1.7° and 6/9 visual acuity. The retina is structured so that the central fovea is dedicated toward high-resolution spatial imaging and the periphery more toward spatiotemporal imaging. The type of vision returned is then dependent on where the electrode is placed.

In practice, numerous issues have impeded the realization of functional retinal prosthesis. Flat implanted chips need to be small within the curvature of the eye, resulting in a tunnel vision. The RGCs connected to the high resolution fovea are bunched up around the macula, meaning that it will be very difficult to return foveal vision. As the number of electrodes starts to scale toward useful vision, power dissipation in the retina can start to become a significant problem [11]. This, in turn, can cause degradation problems in the electrodes themselves. Such problems are the basis for significant investigation, and the general perspective is that rudimentary but increasingly better functioning systems will be available in the coming years.

Manuscript received July 22, 2011; revised October 4, 2011; accepted November 8, 2011. Date of publication November 24, 2011; date of current version March 7, 2013. This work was supported by the Royal Society, the Bioinformatics Research Center, the Engineering Physical Sciences Research Council under Grant F029241, and the European Seventh Framework Programme for funding the OptoNeuro (249867) Research Program. The work of W. Al-Atabany was supported by the Egyptian Government for research funding during the Ph.D. program. *Asterisk indicates corresponding author*.

*W. Al-Atabany is with the Department of Biomedical Engineering, Helwan University, Helwan 11421, Egypt, and also with the School of Electrical, Electronic and Computer Engineering, Newcastle University, Newcastle upon Tyne, NE1 8QB, U.K. (e-mail: walid.al-atabany@h-eng.helwan.edu.eg).

B. McGovern is with the Department of Physics, Imperial College London, London, SW7 2AZ, U.K. (e-mail: brianpatrick.mcgovern@gmail.com).

K. Mehran is with the School of Electrical, Electronic and Computer Engineering, Newcastle University, Newcastle upon Tyne, NE1 8QB, U.K. (e-mail: Kamyar.Mehran@newcastle.ac.uk).

R. Berlinguer-Palmini is with the Institute of Neuroscience, Newcastle University, Newcastle upon Tyne, NE1 8QB, U.K. (e-mail: rolando.berlinguer-palmini@newcastle.ac.uk).

P. Degenaar is with the School of Electrical, Electronic and Computer Engineering, Newcastle University, Newcastle upon Tyne, NE1 8QB, U.K., and also with the Institute of Neuroscience, Newcastle University, Newcastle upon Tyne, NE1 8QB, U.K. (e-mail: Patrick.Degenaar@newcastle.ac.uk).

Color versions of one or more of the figures in this paper are available online at http://ieeexplore.ieee.org.

Digital Object Identifier 10.1109/TBME.2011.2177498

Recently, we have proposed a novel, optogenetic/optoelectronic retinal prosthesis, which offers a solution to some of these challenges [12]. This technology is based on the photosensitization of neurons using light-gated ion channels and pumps, which have been successfully expressed in RGC's [13], bipolar cells [14], and photoreceptors [15]. Such an approach requires high brightness illumination, and we have, therefore, previously presented LED microarray stimulators with up to 4096 pixels [12] with the capacity to scale further.

Optogenetic neural stimulation has, thus far, been demonstrated in primates [16] without negative immune responses. Nevertheless, as RGCs project to the visual cortex, a potential inflammatory response there could have serious negative consequences for the patient. It is, therefore, most likely that early human trials in the coming years will focus on bipolar cells [14] and persisting cones that have lost light sensitivity [15]. Nevertheless, as RP is a progressive disease which also damages these layers, long-term implementation in the RGC layers may also be necessary.

Whichever approach is used, electronic or optogenetic, it is unlikely that we will return perfect vision in the near future. More likely, the resulting vision from a higher resolution retinal prosthesis is likely to have characteristics of both early stage RP patients and age-related macular degeneration (AMD) patients (i.e., tunnel vision with very poor visual acuity). Previously, we have shown that effective contrast enhancement algorithms, such as cartoonization, can improve visual recognition in visually impaired but not blind patients with retinal degenerative disorders [17]. We also demonstrated a seam-assisted shrinkability (SAS) algorithm [18] to spatially compress the nonimportant features of the visual scene, increasing the effective field of view for those having tunnel vision problems.

Additionally, depending on the target retinal layer to be stimulated, some of the retinal processing will have to be performed. Although the retina is complex, the full coding of the exiting different types of RGCs is still under investigation [19]–[21]. However, reduced spatiotemporal models that can be processed in real time on portable platforms may prove sufficient when combined with the plasticity of the brain to adapt interpretation. In this paper, we present the processing platform for a high-resolution optogenetic retinal prosthesis. The scene enhancement algorithms have been incorporated into the system to improve the ability of the patient to use the prosthetic vision to perform visual tasks. To optimize the quality of this prosthetic vision, the platform also includes algorithms that mimic retinal processing to reproduce the ganglion cell spike patterns from healthy retina, taking into account the target neurons and the biophysics of the channelrhodopsin [14]. To ensure that the platform is scalable, we also present a control algorithm to meet the power consumption limitations. As proof of concept, we implemented the platform in a system including camera acquisition and optoelectronic stimulator and demonstrate its use with *ex vivo* preparations.

II. Visual Processing Algorithms

The visual processing is divided into two main parts. In the first part, there are the image enhancement algorithms, which have been developed to enhance the vision of the patient given the small field of view and limited visual acuity.

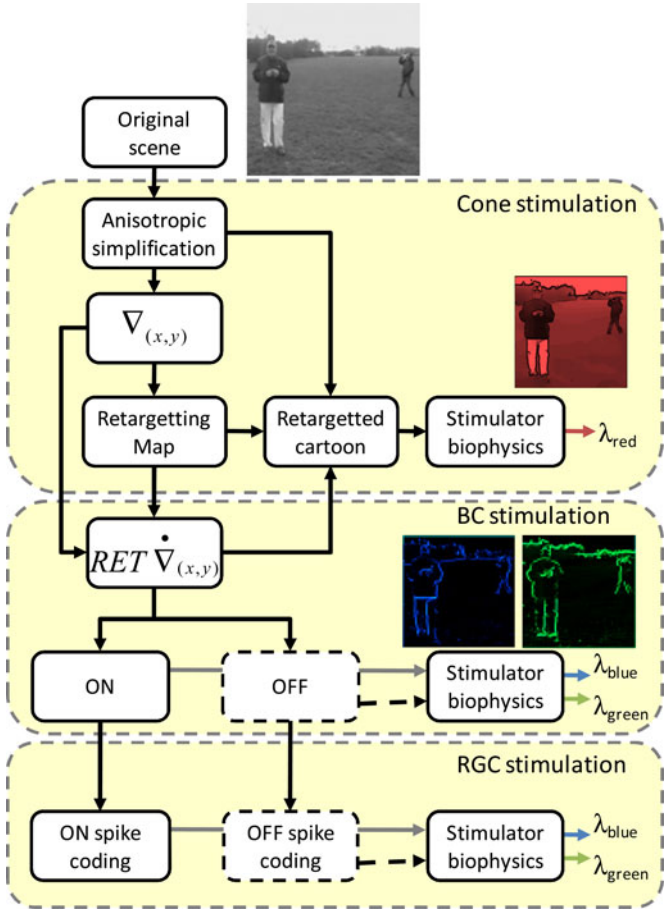

Fig. 1. System flowchart. Main stages of the approach for stimulating different retina targets: resensitized cone, bipolar cell (BC), and RGC stimulation. In the case of cone stimulation, the retargeted simplified cartoon scene will be transmitted. For BC stimulation, both of the retargeted ON and OFF retinal spatiotemporal derivative maps of the scene will be transmitted. Finally, for the RGC stimulation, the SCMs from the spatiotemporal derivatives will be used for stimulation. $\mathrm{RET}\ \dot{\nabla}_{(x,y)}$ represents the retargeted spatiotemporal derivative map.

1) *Scene simplification:* We use anisotropic filtering to simplify the scene, and overlay a negative spatial derivative to complete the effect of cartoonization.
2) *Spatial scene compression:* We develop an importance map from which we dynamically shrink less important features with respect to the important features.

   Second, there are the retinal processing and spike coding algorithms.
3) *Retinal processing:* The algorithms reproduce the ON and (if required) OFF signal pathways in the retina.
4) *Spike coding:* As optogenetic stimulation of RGCs allows control of individual action potentials, we generate a spike coding protocol for both the ON and OFF pathways.

These image processing components are described in the flowchart of Fig. 1. In all cases the first two image enhance-

ment algorithms are applied. The configuration of the rest of the processing platform depends on the target neurons as shown. From the photoreceptors to the optic nerve, signal processing in the retina can be considered to have two main stages, in the outer plexiform layer (OPL) with the interaction of the photoreceptors, the horizontal cells and the bipolar cells, and the inner plexiform layer (IPL) where information from the bipolar cells is processed by the bipolar, amacrine, and RGCs, and transmitted to the brain via the optic nerve. In the case of optogenetic photosensitization of the degenerate cones, where the light sensitive outer segment is nonfunctional or missing but the inner segment retains viability, only the image enhancement algorithms are needed. However, when the bipolar cells are targeted, replication of the OPL retinal processing is needed. Targeting RGC, which has been the approach adopted in prosthesis based on electronic implants, requires the additional IPL processing as well as spike coding. Implementation concerns must also be addressed as the algorithms need to be realized in real time with sufficiently low latency to enable the patient to function effectively, while remaining viable for a portable headset solution and scalable to high resolution.

A. Image Enhancement Algorithms

1) Scene Simplification: Image simplification is an important step before performing the retinal processing. It is also the primarily useful strategy for stimulating optogenetically resensitized cones. The purpose is to suppress nonimportant high frequency noise and textures [22]. As Gaussian smoothing and median filters are not efficient in preserving the significant boundaries in the scene intact, instead, we use an anisotropic diffusion filter. It eliminates noise and low importance textures, while avoiding smoothing across object boundaries. It is an iterative process that progressively smoothes the image while maintaining the significant edges by reducing the diffusivity at those locations having a larger likelihood to be edges [23]. The discrete equation of the anisotropic diffusion filter is

$$I^{n+1} = I^n + \Delta t[\nabla(C \cdot \nabla I_H) + \nabla(C \cdot \nabla I_V) + \nabla(C \cdot \nabla I_{D1}) + \nabla(C \cdot \nabla I_{D2})] \quad (1)$$

where ∇ is the gradient operator and C is the diffusion coefficient or the diffusivity of the equation. *n* denotes the iteration number, Δt is the time step (it controls the accuracy and the speed of the smoothing), and ∇I_H, ∇I_V, ∇I_{D1}, and ∇I_{D2} represent the horizontal (*H*), vertical (*V*), and two diagonal (*D*) gradients of the image. Although there are different methods to calculate the gradients [24], we use Sobel operators for their simplicity in implementation and, thus, processing time/power consumption. Directionless Laplacian filters would require less processing than calculating all four gradients. However, it is more sensitive to fine (irrelevant) textures and produces very thin edges. It is mainly useful in sharpening process. The diffusion coefficient *C* is calculated from the following equation:

$$C = \frac{1}{1 + \sqrt{\nabla I_H^2 + \nabla I_V^2 + \nabla I_{D1}^2 + \nabla I_{D2}^2}}. \quad (2)$$

To increase the visual distinctiveness of high contrast regions in the scene, we overlay a negative spatial derivative over simplified scene that gives a notable edge enhancement giving the image a cartoon like effect. The overlaid spatial derivatives are calculated as follows:

$$\nabla I_X = \nabla I_H + \frac{\nabla I_{D1} + \nabla I_{D2}}{2} \quad (3)$$

$$\nabla I_Y = \nabla I_V + \frac{\nabla I_{D1} - \nabla I_{D2}}{2}. \quad (4)$$

Then, gradient's amplitude is

$$\nabla = \sqrt{\nabla I_X^2 + \nabla I_Y^2}. \quad (5)$$

Patients can control the smoothness or simplification level through increasing or decreasing the number of iterations *n*.

2) Spatial Scene Retargeting: To tackle the tunnel vision problem and the limited resolution of current prosthetic vision systems, we desire to compress the visual scene into the effective field of view. Previous works targeted the process of image compression for retina prosthesis devices depended on ordinary bilinear resizing approach which makes the key features seem further away [25]. This makes the object identification process more difficult at lower spatial resolution. We, therefore, need to nonlinearly retarget the scene into a smaller size, thus expanding the effective field of vision. To do that, we have developed a nonlinear scene retargeting technique, which generates an importance matrix W_{ST}; this involves how much each pixel in the input scene should be nonlinearly shrunk (comprised). It is a combination of two measures: a local saliency gradient map and a temporal motion map. The saliency map comes from (5) and the motion map comes from a temporal derivative of the visual scene

$$W_{\mathrm{ST}} = \nabla(x, y, t) + \frac{1}{n}\sum_{n=1}^{n} \nabla(x, y, t) - \nabla(x, y, t - n). \quad (6)$$

As multiple frames need to be stored in memory and reprocessed, this temporal derivative can be processor intensive. We, therefore, typically use $n = 1$, i.e., the equation then becomes a simple frame difference.

To give higher importance values for the foreground objects over the saliency and background objects, we modify the importance matrix by giving background areas very low importance weights. The modification process starts by looking for seams with lowest cumulative energy values [17], [18]. A seam is defined to be a connecting path of pixels (one in each row, in case of vertical compression) with minimum energy values. This cumulative energy map *M*(*i*,*j*) is generated from the spatiotemporal importance map in the following

$$M(i, j) = W_{\mathrm{ST}}(i, j) + \min[M(i-1, j-1), M(i, j-1), M(i+1, j-1)]. \quad (7)$$

To find the lowest seam energy path, starting from the last row in the cumulative energy matrix M, we search for the minimal cumulative pixel. After that, we work backward from this pixel to obtain an optimal vertical seam by finding the minimum of

the three neighboring pixels of this pixel in the previous row and then store this pixel to the seam path. We do the process of searching for the lowest seam energy path K times, as K is the number of columns to be shrunk. Then, we generate another matrix of size $N \times K$, which contains the x and y positions of the seams. By knowing the locations of lowest energy pixels, we rescale all the pixels of the importance matrix along the path of all the seams to very low importance values.

In order to preserve continuity between rows, $W_{\mathrm{ST}}(i,j)$ should be equal to $W_{\mathrm{ST}}(i-1,j)$, in case of vertical retargeting. For that, we assign a fixed importance value for each column by applying a moving average window of size L and overlapping by $L/2$ on each column in the importance matrix [26]; then, we take the maximum value for each column, so that the updated importance matrix is

$$W(0\colon i_{\max}, j) = \max_{r=1}^{2N/L}\{\bar{W}_r(j)\} \tag{8}$$

where $\bar{W}_r(j)$ is an array containing the moving average values of the importance values in column j.

For dynamic scene retargeting, calculating the importance map for each frame individually generates jittering artifacts in the retargeted video sequence. To counteract this, movement of seams from one scene to the next need to be constrained. We, therefore, calculate the seams of the first couple of frames, and then, the actual locations of these seams are stored into an arbitrary matrix T to be used in calculating the seams for the next frame. These seams' locations are adapted, for the forthcoming frames, if there are dynamics in the scene. If the objects in the frame are static, then the locations of the seams will be the same, but if these objects move, then the seam locations within the same areas through which the objects move around will also move to avoid crossing the moving objects. The adaptation process of the seams locations is fully discussed in our previous paper [18].

As discussed previously, the importance matrix defines which pixels in the source image are significant and should be preserved in the retargeted image. In contrast, the shrinkability matrix defines the relative extent to which pixels in the source image should be shrunk to retarget the image by K columns. The shrinking value of each pixel $S(j)$ in any row, considering retargeting the whole image by only one column, can be calculated from

$$S(j) = \frac{1}{W(j) * \sum_{j=1}^{M} 1/W(j)}. \tag{9}$$

The summation of $S(j)$ over j columns equals 1 if K is 1. Then, we rescale this shrinkage map so that the summation equals to K for higher values of K.

This scaled cumulative shrinkability map is used to retarget the difference of Gaussian (DoG) image to the desired dimension by using an algorithm suggested by Fant [27]. The algorithm is a 1-D method used in separable transformations defined in terms of forward mapping functions. It maps a limited line of discrete input pixel intensity values into a limited line of discrete output pixel intensity value.

B. Retinal Processing

1) Outer Plexiform Layer Processing: The core spatial processing of the horizontal and bipolar cells is the spatial derivative. As the inputs of central cone cells are subtracted from surrounding cone cells, this is classically modeled as a DoG functions. The positive values correspond to the ON pathway and the negative values to the OFF pathway. Each pathway looks similar to a simple edge filtering of the image. We have found slightly better results by combining vertical and horizontal Sobel operators rather than a DoG or Laplacian filter. The resultant time varying spatiotemporal derivative is the one used in (6). However, digitally, the derivative is scaled as an unsigned integer to between -128 and $+128$. Then, the ON signal is, thus, $W_{\mathrm{ST}} > 0$ and the OFF signal is $|W_{\mathrm{ST}} < 0\,|$.

2) Spike Coding: In traditional electronic forms of epiretinal prosthesis, the spiking output from the RGCs has been modulated by stimulation amplitude [28]. Although coding matching the natural output of the retina has been neither attempted nor achieved, patients have seen phosphenes with amplitude roughly correlating to stimulation intensity and, thus, firing frequency. In the case of optogenetic approaches, it is now possible to improve upon this by determining the firing code through pulses of direct optical stimulation.

The coding mathematics of the spike trains that carry the visual information is still under investigation [20], [21]. Primate retina has $\sim$17 RGCs types and the encoding strategies for each of these types are different. Different encoding strategies have been reported in the literature [21]. Generally, these can be classed into rate coding (intensity α number of spikes per second), correlated spike timing (intensity α latency of a spike from an event or other spike), and population coding (information is correlated with neighboring spike patterns) [29]. For example, in response to a step change in local luminance, the firing rate of the midget and parasol cells increases [30]. Meister and Gollisch [20] revealed how the first spike latency on four types of RGCs (particularly fast OFF, biphasic OFF, slow OFF, and fast ON cells) relative to postsaccadic eye movement could encode information. Correlations between multiple ganglion cells spike may constitute another population code, conveying information on the visual stimulus that is not present if ganglion cells acted as independent encoders [31]. However, such correlations in spike timing occur mainly between neighboring ganglion cells which suggests that such synchronization is a local phenomenon. This may be due to shared synaptic inputs [31], [32]. Indeed, other coding schemes could be used; for example, a tonic change in the firing rate of a neuron might represent its response for a small spot. However, in the case of a large spot, the same neuron might respond with oscillatory type firing [29]. Indeed, most of the studies found that the ganglion cells firing rate provides useful information about these stimulus parameters, while the timing of the first action potential provides almost as much information [20], [33].

As spatial synchronization between external μLEDs and a moving eye will be difficult, it will only be possible to chromatically distinguish cell types. Furthermore, with current eye tracking technology, it would be difficult to implement latency

coded to saccadic movements. We, thus, implement a rate-based coding approach. First, we decoded the image intensities into frequencies with an exponentially decaying function. This is defined in the following relation:

$$F(x, y, t) = F_0(x, y) \cdot e^{t/S} \tag{10}$$

where *F(x,y,t)* is the coded frequency for each pixel *I(x,y)*. *S* sets the decay slope profile, which we chose to be $S = 20$ in this study. It can be changed according to the decaying profile of the spike pattern for different RGCs. F_0 is given by

$$F_0(x, y, t) = \frac{f_{\max}}{I_{\max} R(x, y, t)} \tag{11}$$

where $f_{\max}$ is the maximum firing rate of the RGCs, $I_{\max}$ is the maximum intensity of the pixels, and *R(x,y,t)* is the retargeted ON or OFF intensity matrix. Typically, we set $f_{\max} = 40$ Hz which represents the maximum firing frequencies of the tonic firing RGCs that we have previously achieved [12] and $I_{\max} = 255$ which is the maximum unsigned gray level value for any pixel.

Then, *F(x,y,t)* will be a matrix that includes the positions of spikes for each pixel over a time period which we set arbitrarily to 1000 ms. We assume that relaxation of any temporal decay effects will be complete in this time period. The final spike-coded map (SCM) will be a binary matrix that has ones at the position of each spike.

$$\mathrm{SCM}(F(x, y, t)) = 1 \forall \frac{1}{F(x, y, t)} < 1000 \text{ ms}. \tag{12}$$

C. Scalability—Power Control

To stimulate RGC's, we use a GaN LEDs that are capable of emitting high brightness, i.e., emitting over 10 W/cm^2 [34]. As from our previous work [12], we know that the individual microLED emitters operate at around 5 mA to produce enough light to cause an action potential. As 5 W is commonly used as the threshold for fan-assisted cooling, and our operational voltage range is 10 V, we will, therefore, not drive more than 1 A through the chip. This means that each microLED can consume 50 mJ/s; hence, 100 LEDs can be driven simultaneously with such limitations. We calculate that at the resultant irradiance, we would need to pulse for 10 ms to produce an action potential. Therefore, we can drive a total of 10 000 action potentials per second over an array of neurons.

A feasible 1-cm^2 chip could provide around 36 k pixels (192×192 pixels), which was typical for early color mobile telephone screens. The limiting factor on the technological development will be the power requirement, which ultimately limits the number of LEDs that can be illuminated.

One method of limiting the number of pixels to be displayed is to threshold the ON and/or OFF signals. We developed a control algorithm that limits the number of illuminations to 10 000 per second (assuming 10 ms illumination periods). The algorithm limits the number of spikes through exponentially controlling the dynamic range of the scene pixels and by thresholding the pixel intensity value. A set of 15 images ranging from simple to complex scenes has been chosen, and from them we generated two equations for the exponential factor and the threshold value that limit the summation of the spikes to 10 000

$$E = A_E e^{\alpha S} - B_E e^{\beta S} - C_E \tag{13}$$

$$T = A_T e^{\alpha S} - B_T e^{\beta S} - C_T \tag{14}$$

where E and T are the exponential factor and the intensity threshold values, respectively. S represents the summation of the preprocessed spatiotemporal derivative intensities, and the constants have the following values:

	A	B	C	α	β
E	0.85	356.8	0.12	0.0003	-0.0134
T	0.21	103.6	0.03		

Then, for a given point in time, the dynamically scaled and retinally processed and thresholded image will be

$$\text{Scaled } \dot{\nabla}_{(x,y)} = e^{E \cdot \dot{\nabla}_{(x,y)}} \tag{15}$$

$$\text{Thresholded } \dot{\nabla}_{(x,y)} = \begin{cases} \text{Scaled } \dot{\nabla}_{(x,y)} & \text{if} > T \\ 0 & \text{if} < T \end{cases}. \tag{16}$$

As aforementioned, from previous data, the maximum spike rate that can be reliably generated at the RGC's is 40 Hz. Given that the RGCs need at least two spikes to recognize the pixel value at a certain frame, the maximum frame rate that can be sent to these cells is 10 frames/s. This means that the minimum grayscale intensity value that we can encode at each frame is 104 (if we have 256 grayscale levels), which represents a spike with frequency of 99 Hz. To encode the video stream, we encode the pixels of each frame over a period of 100 ms at maximum and the position of last spike for each pixel is stored to be the starting point from which the spikes for the next frame will start.

D. Implementation

Key to this long-term system is its implementability into a portable and wearable head-mounted display (HMD) system. The prototyping platform that can be connected to the LED unit is implemented on a MATLAB platform on a desktop computer; with a 2.8-GHz Intel core quad processor, 8-Gb memory, and a GTX285 graphics card. To utilize the parallel processing power of the graphics card, the scene simplification, retina processing, and spike coding processes are implemented using the AccelerEyes graphics processing unit (GPU) jacket plug-in [35] for MATLAB. The scene retargeting process which is a more linear operation is processed on the CPU/floating point unit.

As our target is to implement this system on a portable platform, we implemented the scene simplification and spatiotemporal derivative processes on a Tegra I development platform from NVidia [6]. The Tegra I is a system-on-a-chip platform with an ARM CPU core and a graphics processor with eight processing cores. There is a feed from the camera to the GPU allowing power efficient parallel processing. The specification of the Tegra I is low compared to laptop or desktop processors. However, the CPU/GPU operations can be performed at sub-1W power consumption which is desirable for portable/wearable processing. We also calculated estimated improvements for speed for the Tegra II and III platforms according to NVidia's specifications.

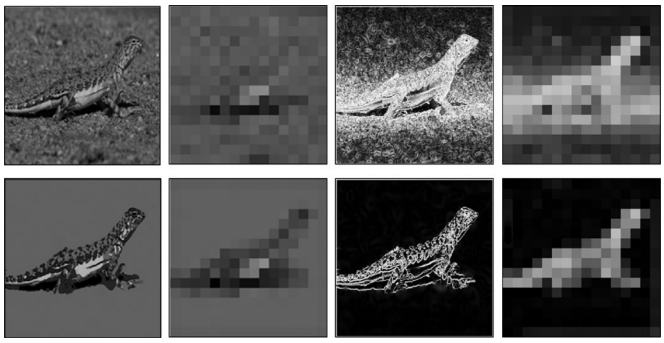

Fig. 2. Effect of scene simplification in reducing irrelevant information. (Top row from left to right) 256 × 256 and 16 × 16 pixels scene of a lizard on a low contrast background, 256 × 256 and 16 × 16 pixels versions of subsequent retinal processing (ON image). (Bottom row) Cartoonized scene at 256 × 256 and 16 × 16 pixels and subsequent retinal processing.

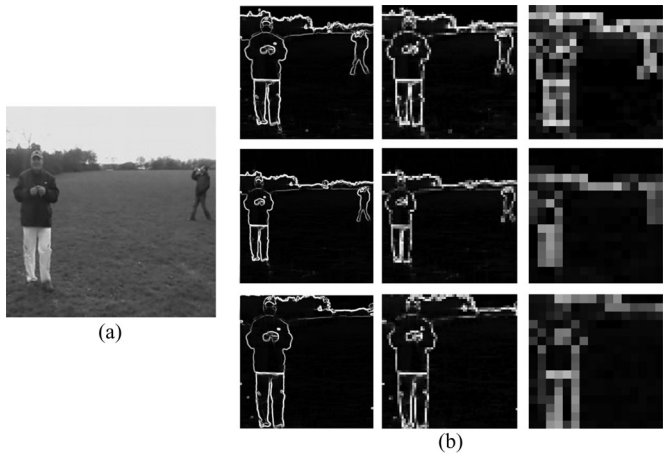

Fig. 3. (a) and (b) Effect of different retargeting techniques with respect to retargeted image size. (From left to right) First, second, and third rows show the retargeted image to 256 × 256, 64 × 64 and 16 × 16 when using our retargeting, simple bilinear resizing, and cropping methods, respectively.

III. Results

A. Scene Simplification

To demonstrate the effect of scene simplification, the retinal processing (spatial derivative) was calculated for an original image and a cartoonized version. The images are scaled to 256 × 256, and 16 × 16, respectively, to show the effect over different resolutions. As shown from the bottom row in Fig. 2, scene simplification removed low importance textures while keeping the relevant boundaries intact.

The effect is also striking for spatiotemporal processing (data not shown). By simplifying the scene, the key features—in this case a lizard on a low contrast background—are enhanced. This effect is scalable across resolutions and is also striking for spatiotemporal processing (data not shown). Additionally, with texture removal, it reduces the total information to be sent to the LEDs and makes it easier to threshold.

B. Spatial Scene Compression

Fig. 3 shows a snapshot from video file for subjects moving in playground field with dimension of 400 × 400. The scene is retargeted using three methods: our SAS retargeting approach [the first row in Fig. 3(b)], bilinear resizing (second row), and cropping (last row). The SAS method cannot know future scenes, so it exhibits an increasing wobble or video jitter with higher spatial compressions. Subjectively, we find that a 25–40% compression gives the most effective result [18]. We, therefore, show comparative compressed images of 256 × 256 pixels for each of the cases, which are then interpolated to 64 × 64 and 16 × 16 pixels.

Image cropping simply uses the scene as it is and represents the effects of tunnel vision. In this example, the viewer can see the person on the left but not on the right within the same scene. Bilinear resizing demagnifies the scene, so the key features will seem further away. As they will then be at lower spatial resolution, it will be harder to identify them. The SAS algorithm compresses the less useful information keeping the main features at the same size. As can be seen from the images, the effect is subtle. The person on the left and right are 25% larger than they would be for dignified images. In static images, it does not appear so different, but for dynamic scenes, it can affect time for recognition in patients as declared in our previous paper [18]. In the literature, there is also work by Peli *et al*. [36] that overlays a compressed edge form of the scene onto the image in the tunnel. Although it might be useful in augmented vision systems, but this would form too complex image to be useful for retinal prosthesis systems.

C. Stimulator Biophysics

Our LED stimulator is pulse modulated. For intensity modulation (cone, bipolar cell stimulation), we simply vary the pulse within the cells integral period (∼20 ms). We, therefore, focus our attention on the spike-coded stimulation of the RGCs. Fig. 4 shows the scalability of the spike coding algorithm through generating SCMs for the scene shown in Fig. 3 between 16 × 16 and 256 × 256. We assume in the first instance that only the ON matrix will be transferred, as to date, the only genetic specificity to be achieved has been for ON bipolar cells [14]. The bottom row shows the bipolar ON importance matrix, the middle row shows a histogram of the number of LEDs that are ON, and the top row shows a snapshot of the spiking profile. From this figure, we can see that the uniformity of the spiking histogram shows the optimum use of the LED array.

At present, the pulse width is determined by the brightness/efficiency of the microLED stimulator and the efficiency of the channelrhodopsin. Already a CatCh [37] form of channelrhodopsin shows significantly improved light requirement and we expect further improvements in the coming years. Similarly, we expect to improve the external quantum efficiency of the microLED stimulator. In practice, this will reduce the required stimulation pulse width. Reducing the width of the stimulating pulse increases the number of the allowed stimulating spikes. This, in turn, enhances the visual perceived scene for larger image sizes (e.g., 256 × 256).

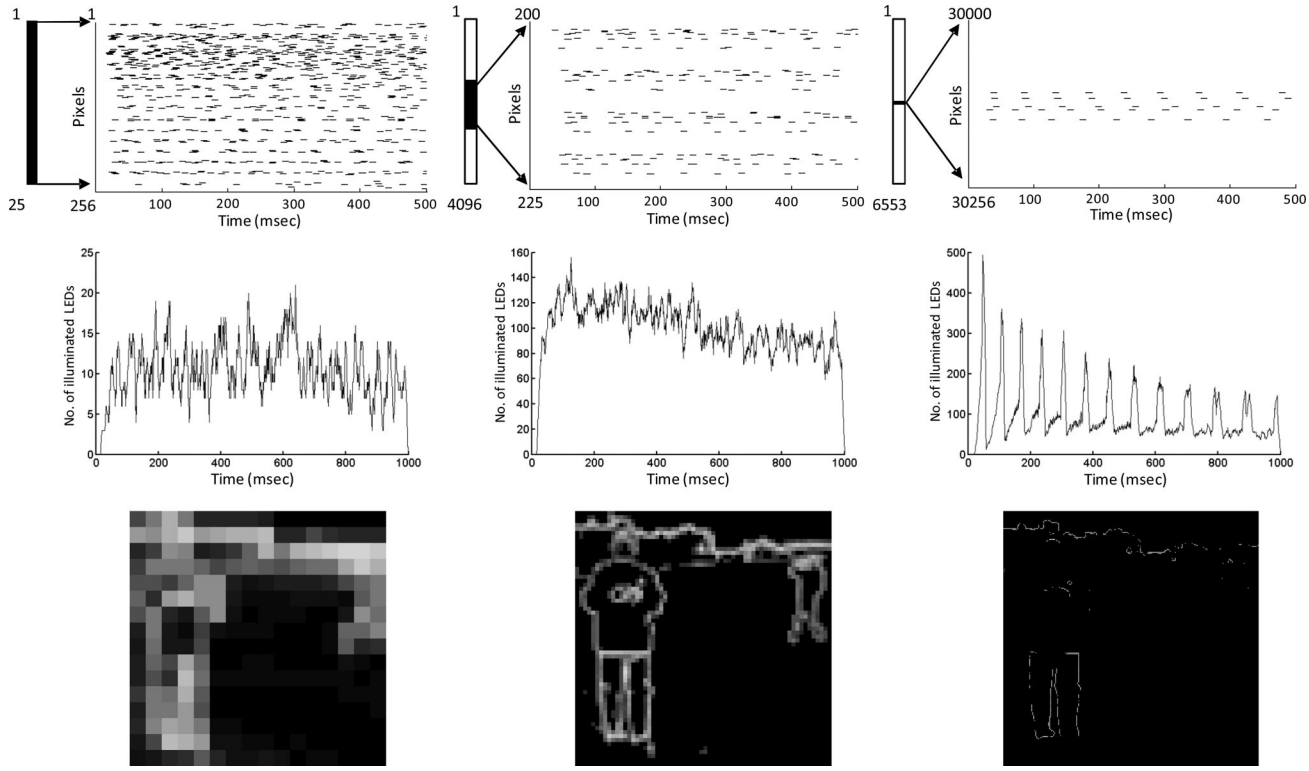

Fig. 4. SCMs for the scene shown in Fig. 3 and the corresponding LEDs' histogram. (From right to left) Spike maps for the 16 × 16, 64 × 64, and 256 × 256 retargeted image. The histograms of the number of LEDs that are ON are shown in the middle row for each scale, respectively. The integrations of the spikes over 1000 ms are shown in the last row for each scale, respectively, considering that the maximum number of illuminated LED per second is 100 000.

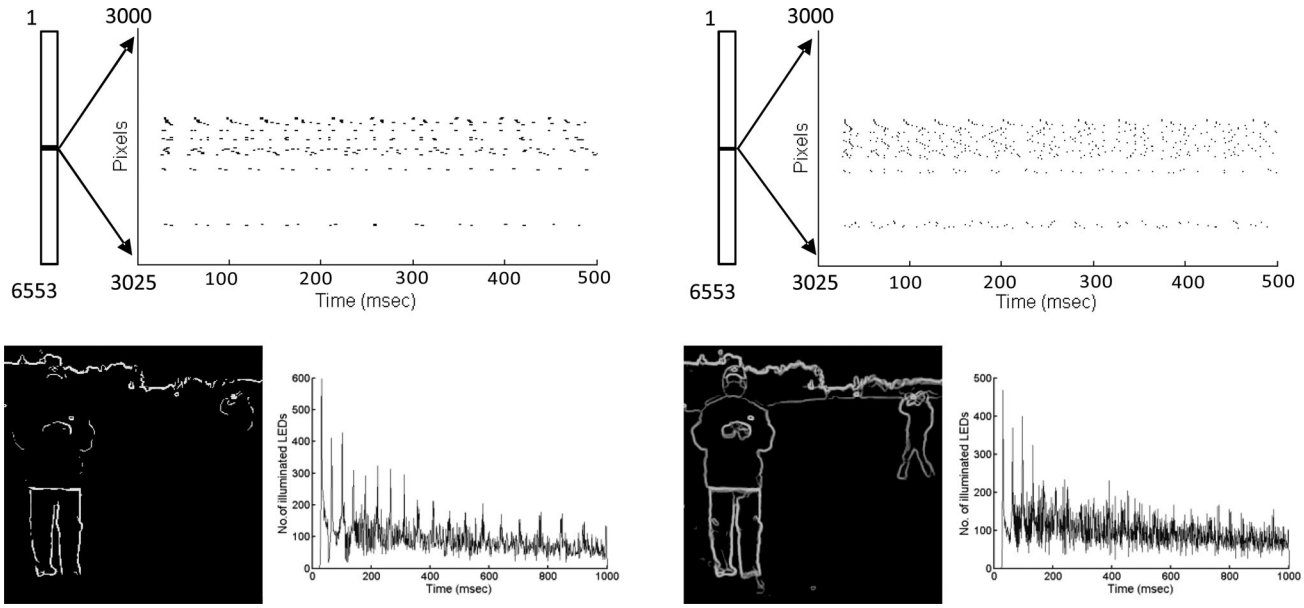

Fig. 5. Effect of reducing the spike width. (Top row) SCMs for an image of 256 × 256 pixels in case of reducing the spike width into (left) 3 ms and (right) 1 ms. The images reconstructed from integrating the spikes and the histograms of the number of LEDs are shown in the bottom row.

Fig. 5 shows the SCMs for a 256 × 256 image with two different pulse width: 3 and 1 ms, respectively. Comparing this with Fig. 4 (in which the pulse width is 10 ms), we can see that at higher frame size (e.g., 256 × 256), only pixels of high intensity values are transmitted so that the histogram takes an exponentially decaying and periodic shape. At lower pulse widths (3 and 1 ms), more pixels can be kept, and hence, more spikes can be generated from them. The histogram profile will also be flattened as shown in Fig. 5 (bottom row).

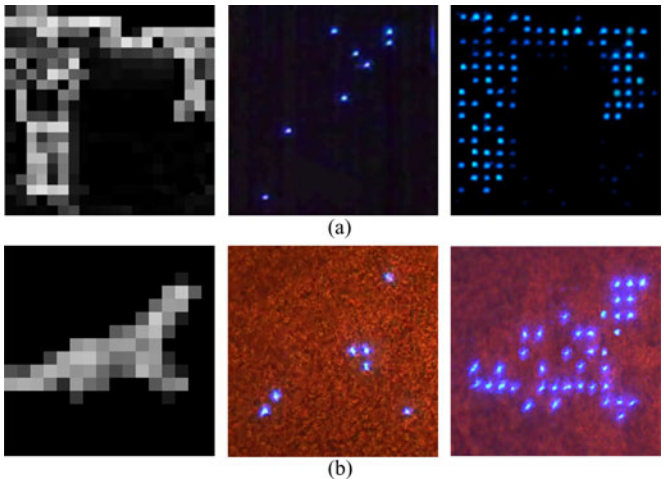

Fig. 6. Real spikes recorded from the microLEDs chip for two different scenes. (Left column) Real 16×16 images before the conversion into spikes and sending them to the chip. (Middle column) Snapshot recorded from the chip. (Right column) Integration of all the recorded frames that reconstruct the original scenes. (Bottom row) Image shone onto a real mouse retina.

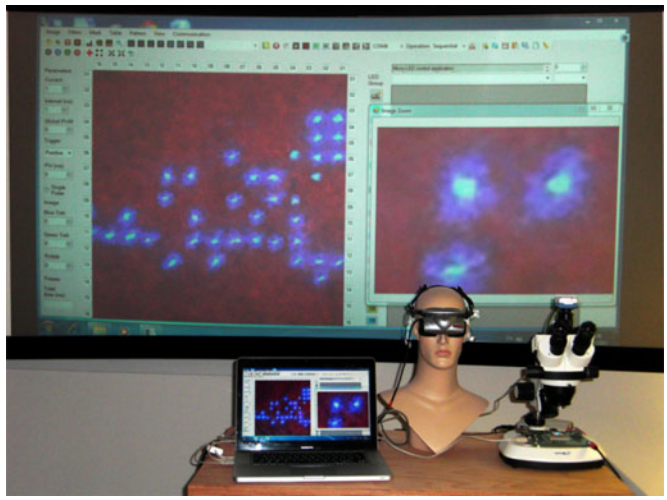

Fig. 7. Snapshot from the experiment, a snapshot for the whole system describing the main components. (Left) Computer system performing the processing. (Center) Virtual reality helmet camera on a dummy. (Right) MicroLEDs analyzed under a microscope.

D. Implementation

Fig. 6 shows the final output on a matrix addressed LED chip [34]. The chip is outputting the scenes as shown in Figs. 2 and 3. These represent both simple and complex scenes, respectively. The spikes were transferred to the chip with an extended period (100 s rather than 1 s), as our camera acquisition could only take frames at 40-ms intervals. A single frame is shown in the centre image. We then integrated the intensity output over the entire period, recording from all 1000 spike frames. The reconstructed scene is shown on the right after being integrated from both the chip directly (top) and from real mouse retina (bottom). The preparation of the mouse retina followed the following steps; a neonatal C57BL/6 mouse pup was euthanized by cervical dislocation and enucleated before retinal isolation. The isolated retina was then transferred to the experimental chamber and placed, RGC layer facing down, onto a CMOS-based large-scale high-resolution microelectrode array platform with full frame acquisition consisting of 4096 electrodes (21 μm per side) arranged in a 64×64 grid and tightly packed (pitch of 42 μm). The retina was kept at 32 °C and continuously perfused (0.5–1 mL/min) with artificial cerebrospinal fluid containing the following (in millimolar): 118 NaCl, 25 $NaHCO_3$, 1 $NaH_2\ PO_4$, 3 KCl, 1 $MgCl_2$, 2 $CaCl_2$, and 10 glucose, equilibrated with 95% O_2 and 5% CO_2. All animal procedures were conducted under the U.K. Home Office, Animals (Scientific Procedures) Act 1986. The microLEDs array was imaged onto the retina by means of a dissecting stereomicroscope (VWR).

A snapshot of the experiment is shown in Fig. 7 which shows a camera fixed on a HMD helmet that captures the visual scene and transfers it into a portable laptop. Then, the captured scene is digitally processed and converted into spikes (in the case of RGCs stimulation) to the LED chip.

In the virtual reality community, the commonly accepted target for video implementation needs to be at 50 frames/s with 1 frame or less latency to prevent motion sickness and eye strain. This is due to the peripheral vision acquiring visual information faster than the central vision. It can be difficult to obtain imaging systems that achieve this, and in the case of retinal prosthesis, especially for tunnel vision effects, the target is perhaps overly stringent. Nevertheless, it is a good point of reference.

Since this study began, there have been further improvements in the performance of mobile GPU systems. Notably, a third generation Tegra device has been announced with double the number of GPU cores and an expected performance improvement of 4X [38]. We fully expect to be able to achieve all our algorithms close to video rate under such portable system.

IV. Discussion

In this paper, we present a full processing solution for retinal prosthesis. Our focus is on optogenetic approaches, but the image enhancement and retinal processing are also applicable to electronic approaches. One significant feature with the optogenetic approach is that it does not require implantation. A viral injection could be administered in similar fashion to antivascular endothelial growth factor treatments for wet AMD. The patient could then wear an optoelectronic stimulator using existing virtual reality headset optics. As there is no expensive surgery, the stimulator headset will become one of the most significant cost factors. It is, therefore, our feeling that the use of mobile GPU processing platforms can provide sufficient power/performance characteristics at significantly lower cost than dedicated CMOS chip solutions.

Our results showed the importance of scene simplification and retargeting approaches before coding the scene into spikes. We also demonstrated how (assuming retinal coding) the image sent to the patient will scale with increasing resolution and decreasing irradiance requirements. We believe both will occur in tandem.

Seasickness in healthy subjects using virtual reality headsets has previously been reported [38], [39]. This is generally

assumed to be due to latency between head movement and perceived image, but affects some more than others. However, it is not yet clear how this can affect the prosthetic vision for blind subjects, and will need to be assessed in patient trials. In the previous study, we were concerned on how the jittering effect of our scene retargeting approach can be acceptable and whether it could cause undesirable effects such as seasickness. We have only tested using augmented reality approaches in healthy subjects for short periods of time. However, we concluded that, subjectively, a 25–40% compression from the original size can give acceptable results [18]. No seasickness was reported amongst our trailers.

We hypothesize that the returned vision of those receiving a prosthetic vision system will be quite different to our own, and such discussions really need to be tested in patients using the device chronically. It may be that, during navigation, patients may have to minimize the use of retargeting due significant head movements relative to the scene. Then, at stationary, the reverse may be the case. For example, with current technology, optical telescopes are used to help distance visual acuity by AMD patients. It is not comfortable to walk looking through a telescope but patients use it when necessary, e.g., to see bus numbers when standing at the bus stop. However, this issue needs to be tested on real tunnel vision subjects.

We demonstrated the output on our individually addressable 16×16 microLED array, which had pixel sizes of 150×150 μm. We are now scaling this up to chip sizes of 1 cm $\times$ 1 cm. If we simply scaled the present array, we would achieve a $64\times$ 64 pixel array. However, as there is a considerable potential for miniaturizing the pixel size, we should be able to achieve higher resolutions. The limiting factor on the technological development will be the power requirement, which ultimately limits the number of illuminated LEDs. This is reflected in our algorithms. Whether we use shorter higher intensity pulses or longer lower intensity pulses, the power consumption by the LEDs will be the same (assuming equivalent efficiency that is actually nonlinear).

We have implemented a spike coding scheme based on a decaying rate coded scheme. Technical and physiological limitations presently limit us from replicating each RGC response for different types of stimuli. As genetic targeting technologies improve, and eye tracker technologies improve, it will be possible to chromatically encode specific cell types [14] and perform latency coding related to eye movements [20].

We have demonstrated that our algorithms can be implemented on PC's, laptops, and mobile phone processing platforms. Our nonoptimized code achieved close to video rate on former. With further developments in mobile processing platforms, we are confident that our algorithms can be implemented at video rate. The estimated power consumption is around 1 W, which is similar to the requirements of the LED units. A typical mobile phone battery is capable of $\sim$5 Wh. Three perhaps four such batteries would power the required processing over the course of a day. As the LEDs require more power, this will be more of a challenge (bigger more bulky batteries). There will, therefore, be an interesting trade-off in the future between battery life and image quality. But again, as the efficiency of both the microLED illuminator and the channelrhodopsin biophysics improves, the power requirement will be decreased.

We finally note that there are some missing pixels in the reconstructed scenes, as the bump bonding between our first-generation microLED devices and controlling electronics are not perfect (see Fig. 6). We expect this to improve with better fabrication techniques in future.

V. Conclusion

We have shown, in this paper, the scene preprocessing steps needed to be used in an *in vitro* system to stimulate arrays of genetically engineered nerve cells using light. The aim of this preprocessing is to enhance and maximize the visual information included in the scene before spike coding and sending it to the retina. We demonstrated how the scene simplification and our nonlinearly retargeting technique kept the relevant information of the scene when it is downscaled to small scales. Also, we showed that the spike coding control program controls the number of illuminated LEDs based on the information that a 10 ms of illumination is needed to produce an action potential. However, if this duration is reduced, then more information can be encoded and sent to the retina.

References

[1] M. S. Humayun, J. D. Dorn, A. K. Ahuja, A. Caspi, E. Filley, G. Dagnelie, J. Salzmann, A. Santos, J. Duncan, L. daCruz, S. Mohand-Said, D. Elliot, M. J. McMahon, and R. J. Greenberg, "Preliminary 6 month results from the argus (TM) II epiretinal prosthesis feasibility study," in *Proc. Annu. Int. Conf. IEEE Eng. Med. Biol. Soc.*, 2009, vol. 1–20, pp. 4566–4568.

[2] E. Zrenner, K. U. Bartz-Schmidt, H. Benav, D. Besch, A. Bruckmann, V.-P. Gabel, F. Gekeler, U. Greppmaier, A. Harscher, S. Kibbel, J. Koch, A. Kusnyerik, T. Peters, K. Sting, H. Sach, A. Stett, P. Szurman, B. Wilhelm, and R. Wilke, "Subretinal electronic chips allow blind patients to read letters and combine them to words," in *Proc. Roy. Soc. B-Biol. Sci.*, May 22, 2011, vol. 278, pp. 1489–1497.

[3] C. Hamel, "Retinitis pigmentosa," *Orphanet J. Rare Diseases*, vol. 1:40, Oct. 2006.

[4] M. A. Musarella and I. M. Macdonald, "Current concepts in the treatment of retinitis pigmentosa," *J. Ophthalmol.*, vol. 2011, ID 753547, 2011.

[5] A. V. Cideciyan, T. S. Aleman, S. L. Boye, S. B. Schwartz, S. Kaushal, A. J. Roman, J.-J. Pang, A. Sumaroka, E. A. M. Windsor, J. M. Wilson, T. R. Flotte, G. A. Fishman, E. Heon, E. M. Stone, B. J. Byrne, S. G. Jacobson, and W. W. Hauswirth, "Human gene therapy for RPE65 isomerase deficiency activates the retinoid cycle of vision but with slow rod kinetics," in *Proc. Nat. Acad. Sci. USA*, Sep. 30, 2008, vol. 105, pp. 15112–15117.

[6] M. H. Tan, A. J. Smith, B. Pawlyk, X. Xu, X. Liu, J. B. Bainbridge, M. Basche, J. McIntosh, H. V. Tran, A. Nathwani, T. Li, and R. R. Ali, "Gene therapy for retinitis pigmentosa and Leber congenital amaurosis caused by defects in AIPL1: Effective rescue of mouse models of partial and complete Aipl1 deficiency using AAV2/2 and AAV2/8 vectors," *Human Molecular Genetics*, vol. 18, pp. 2099–2114, Jun. 15, 2009.

[7] J. L. Stone, W. E. Barlow, M. S. Humayun, E. de Juan, Jr., and A. H. Milan, "Morphometric analysis of macular photoreceptors and ganglion-cells in retinas with retinitis-pigmentosa," *Arch. Ophthalmol.*, vol. 110, pp. 1634–1639, Nov. 1992.

[8] G. J. Chader, J. Weiland, and M. S. Humayun, "Artificial vision: Needs, functioning, and testing of a retinal electronic prosthesis," *Prog. Brain Res.*, vol. 175, pp. 317–332, 2009.

[9] K. Cha, K. W. Horch, and R. A. Normann, "Mobility performance with a pixelized vision system," *Vision Res.*, vol. 32, pp. 1367–1372, 1992.

[10] K. H. Cha, K. W. Horch, and R. A. Normann, "Simulation of a phosphene-based visual-field - visual-acuity in a pixelized vision system," *Ann. Biomed. Eng.*, vol. 20, pp. 439–449, 1992.

[11] C. de Balthasar, S. Patel, A. Roy, R. Freda, S. Greenwald, A. Horsager, M. Mahadevappa, D. Yanai, M. J. McMahon, M. S. Humayun, R. J. Greenberg, J. D. Weiland, and I. Fine, "Factors affecting perceptual thresholds in epiretinal prostheses," *Investigative Ophthalmol. Visual Sci.*, vol. 49, pp. 2303–2314, Jun. 2008.
[12] P. Degenaar, N. Grossman, M. A. Memon, J. Burrone, M. Dawson, E. Drakakis, M. Neil, and K. Nikolic, "Optobionic vision–a new genetically enhanced light on retinal prosthesis," *J. Neural. Eng.*, vol. 6, no. 3, 035007, Jun. 2009.
[13] A. D. Bi, J. Cui, Y.-P. Ma, E. Olshevskaya, M. Pu, A. M. Dizhoor, and Z. H. Pan, "Ectopic expression of a microbial-type rhodopsin restores visual responses in mice with photoreceptor degeneration," *Neuron*, vol. 50, pp. 23–33, Apr. 6, 2006.
[14] P. S. Lagali, D. Bayla, G. B. Awatramani, T. A. Munch, D. S. Kim, V. Busskamp, C. L. Cepko, and B. Roska, "Light-activated channels targeted to ON bipolar cells restore visual function in retinal degeneration," *Nature Neurosci.*, vol. 11, pp. 667–675, Jun. 2008.
[15] V. Busskamp, J. Duebel, D. Balya, M. Fradot, T. M. Viney, S. Siegert, A. C. Groner, E. Cabuy, V. Forster, M. Seeliger, M. Biel, P. Humphries, M. Paques, S. Mohand-Said, D. Trono, K. Deisseroth, J. A. Sahel, S. Picaud, and B. Roska, "Genetic reactivation of cone photoreceptors restores visual responses in retinitis pigmentosa," *Science*, vol. 329, pp. 413–417, Jul. 23, 2010.
[16] X. Han, X. Qian, J. G. Bernstein, H. H. Zhou, G. T. Franzesi, P. Stern, R. T. Bronson, A. M. Graybiel, R. Desimone, and E. S. Boyden, "Millisecond-timescale optical control of neural dynamics in the nonhuman primate brain," *Neuron*, vol. 62, pp. 191–198, Apr. 30, 2009.
[17] W. Al-Atabany, M. A. Memon, S. M. Downes, and P. A. Degenaar, "Designing and testing scene enhancement algorithms for patients with retina degenerative disorders," *BioMed. Eng. OnLine*, vol. 9:27, 2010.
[18] W. Al-Atabany, T. Tong, and P. A. Degenaar, "Improved content aware scene retargeting for retinitis pigmentosa patients," *BioMed. Eng. OnLine*, vol. 9:52, 2010.
[19] G. D. Field and E. J. Chichilnisky, "Information processing in the primate retina: Circuitry and coding," *Annu. Rev. Neurosci.*, vol. 30, pp. 1–30, 2007.
[20] M. Meister and T. Gollisch, "Rapid neural coding in the retina with relative spike latencies," *Science*, vol. 319, pp. 1108–1111, Feb. 22, 2008.
[21] D. K. Freeman, J. F. Rizzo, III, and S. I. Fried, "Encoding visual information in retinal ganglion cells with prosthetic stimulation," *J. Neural Eng.*, vol. 8, no. 3, 035005, Jun. 2011.
[22] W. Atabany and P. Degenaar, "A robust edge enhancement approach for low vision patients using scene simplification," in *Proc. Cairo Int. Biomed. Eng. Conf.*, 2008, pp. 1–4.
[23] P. Perona and J. Malik, "Scale-space and edge-detection using anisotropic diffusion," *IEEE Trans. Pattern Anal. Mach. Intell.*, vol. 12, no. 7, pp. 629–639, Jul. 1990.
[24] M. Sharifi, M. Fathy, and M. T. Mahmoudi, "A classified and comparative study of edge detection algorithms," in *Proc. Int. Conf. Inf. Technol.: Coding Comput.*, 2002, pp. 117–120.
[25] N. Sharmili, P. S. Ramaiah, and G. Swamynadhan, "Image compression and resizing for retinal implant in bionic eye," *Int. J. Comput. Sci. Eng. Survey*, vol. 2, pp. 30–37, 2011.
[26] A. C. Bovik, *Handbook of Image and Video Processing*. Orlando, FL: Academic, 2005.
[27] K. M. Fant, "A nonaliasing, real-time spatial transform technique," *IEEE Comput. Graphics Appl.*, vol. 6, no. 1, pp. 71–80, Jan. 1986.
[28] J. D. Weiland, W. Liu, and M.S. Humayun, "Retinal prosthesis," *Annu. Rev. Biomed. Eng.*, vol. 7, pp. 361–401, 2005.
[29] J. D. Victor, "Temporal aspects of neural coding in the retina and lateral geniculate," *Network-Comput. Neural Syst.*, vol. 10, pp. R1–R66, Nov. 1999.
[30] J. B. Troy and T. Shou, "The receptive fields of cat retinal ganglion cells in physiological and pathological states: Where we are after half a century of research," *Prog. Retinal Eye Res.*, vol. 21, pp. 263–302, 2002.
[31] J. Shlens, F. Rieke, and E. Chichilnisky, "Synchronized firing in the retina," *Current Opin. Neurobiol.*, vol. 18, pp. 396–402, Aug. 2008.
[32] F. Rieke and P. K. Trong, "Origin of correlated activity between parasol retinal ganglion cells," *Nature Neurosci.*, vol. 11, pp. 1343–1351, Nov. 2008.
[33] E. Fernandez, J. Ferrandez, J. Ammermuller, and R. A. Normann, "Population coding in spike trains of simultaneously recorded retinal ganglion cells," *Brain Res.*, vol. 887, pp. 222–229, Dec. 22, 2000.
[34] B. McGovern, R. B. Palmini, N. Grossman, E. Drakakis, V. Poher, M. Neil, and P. Degenaar, "A new individually addressable micro-LED array for photogenetic neural stimulation," *IEEE Trans. Biomed. Circuits Syst.*, vol. 4, no. 6, pp. 469–476, Dec. 2010.
[35] J. Kong, M. Dimitrov, Y. Yang, J. Liyanage, L. Cao, J. Staples, M. Mantor, and H. Zhou, "Accelerating MATLAB image processing toolbox functions on GPUs," presented at the 3rd Workshop Gen.-Purpose Comput. Graphics Process. Units, Pittsburgh, PA, 2010.
[36] E. Peli, G. Luo, A. Bowers, and N. Rensing, "Invited paper: Augmented vision head-mounted systems for vision impairments," in *Proc. SID Int. Symp. Dig. Tech. Papers*, 2007, vol. 38, pp. 1074–1077.
[37] S. Kleinlogel, K. Feldbauer, R. E. Dempski, H. Fotis, P. G. Wood, C. Bamann, and E. Bamberg, "Ultra light-sensitive and fast neuronal activation with the Ca(2+)-permeable channelrhodopsin CatCh," *Nature Neurosci.*, vol. 14, pp. U513–U152, Apr. 2011.
[38] Joseph J. LaViola, Jr., "A discussion of cybersickness in virtual environments," *SIGCHI Bull.*, vol. 32, pp. 47–56, 2000.
[39] R. H. Y. So and W. T. Lo, "Cybersickness: An experimental study to isolate the effects of rotational scene oscillations," in *Proc. IEEE Virtual Reality*, 1999, pp. 237–241.

Walid Al-Atabany received the B.Sc. and M.Sc. degrees from the Department of Biomedical Engineering, Cairo University, Giza, Egypt, in 1999 and 2004, respectively, and the Ph.D. degree in biomedical engineering from Imperial College London, London, U.K. in 2010.

He is currently a Research Associate in the School of Electrical, Electronic and Computing Engineering, Newcastle University, Newcastle upon Tyne, U.K. He is also with the Department of Biomedical Engineering, Helwan University, Helwan, Egypt.

Brian McGovern received the B.Eng. degree in electrical and electronic Engineering, the M.Sc. degree in electronics, and the Ph.D. degree in VLSI array processors all from the Queen's University Belfast, Belfast, U.K., in 1988, 1989, and 1993, respectively, and the B.Sc. degree in optometry from the City University London, London, U.K., in 2006.

He is a qualified optometrist and is currently with the Department of Physics, Imperial College London, London. His research interests include the area of vision and visual systems, both human and computer and neurobionics.

Kamyar Mehran received the B.Sc. degree in computer engineering in 1998, and the M.Sc. and Ph.D. degrees in control and artificial intelligence in 2010 all from Newcastle University, Newcastle upon Tyne, U.K.

He is currently with the School of Electrical, Electronic and Computing Engineering, Newcastle University. His previous professional experience was mainly on software development. His current research interest is focused on developing algorithms and software interface to robustly control sizable array of ultrabright microLEDs.

Rolando Berlinguer-Palmini received the M.Sc. degree in molecular biology and the Ph.D. degree in physiological sciences from the University of Florence, Florence, Italy, in 1998 and 2004, respectively.

He was in the Department of Pharmacology, University of Florence, studying stroke and mood disorders, for four years. He is currently a Research Associate at the Institute of Neuroscience, Newcastle University, Newcastle upon Tyne, U.K.

Patrick Degenaar received the B.Sc. (first class Hons.) in applied physics and the M.Res. degree in surface science from the University of Liverpool, Liverpool, U.K.. He received the Ph.D. degree in bioelectronics and bioimaging from the Japan Advanced Institute of Science and Technology, Ishikawa, Japan, in 2001.

He is a Senior Lecturer in biomedical engineering in the School of Electrical, Electronic and Computer Engineering, Newcastle University, Newcastle upon Tyne, U.K. He is also with the Institute of Neuroscience, Newcastle University. His research interests include the development of optogenetic retinal prosthesis for the visually impaired.